Available online at www.sciencedirect.com

jmr&t Journal of Materials Research and Technology

journal homepage: www.elsevier.com/locate/jmrt

Structural, mechanical and tribological performance of a nano structured biomaterial Co–Cr–Mo alloy synthesized via mechanical alloying

Mamoun Fellah [a,*], *Naouel Hezil* [b], *Dikra Bouras* [c], *Aleksei Obrosov* [d,**], *Abdul Samad Mohammed* [e], *Alex Montagne* [f], *Assmaa Abd-Elmonem* [g], *Sayed M El Din* [h], *Sabine Weiß* [d]

[a] *Mechanical Engineering Department, ABBES Laghrour-University, Khenchela, P.O 1252, 40004, Algeria*
[b] *Matter Sciences Department, ABBES Laghrour – University, Khenchela P.O 1252, 40004, Algeria*
[c] *Larbi Ben M'Hidi University, Oum El Bouaghi, 04000, Algeria*
[d] *Department of Physical Metallurgy and Materials Technology, Brandenburg Technical University, 03046, Cottbus, Germany*
[e] *Mechanical Engineering Department & IRC-AM, King Fhad University of Petroleum and Minerals, Dhahran, 31261, Saudi Arabia*
[f] *LAMIH Univ Polytechnique Hauts-de-France, UMR 8201, F-59313 Valenciennes, France*
[g] *Departement of Mathematics, College of Science, King Khalid University, Abha, Saudi Arabia*
[h] *Centre of Research, Faculty of Engineering, Future University in Egypt New Cairo 11835, Egypt*

ARTICLE INFO

Article history:
Received 2 April 2023
Accepted 3 June 2023
Available online 9 June 2023

Keywords:
Tribology
Wear resistance
Friction
Powder metallurgy
Co–Cr–Mo alloy

ABSTRACT

The influence of milling time on the tribological behavior of a Co–Cr–Mo alloy designed for biomedical applications, synthesized via mechanical alloying is investigated. Elemental Co, Cr and Mo powders are milled using different milling times (2, 6, 12 and 18 h) in a high-energy ball mill. The resulting powders were subjected to cold uniaxial and hot isostatic pressing respectively, followed by sintering to obtain cylindrical samples, which were evaluated for their structural, mechanical and the wear behavior. Results showed that the grain and crystallite sizes of the powders decreased with increasing milling time, reaching low values of <10 μm and 32 μm respectively, at higher milling times. Furthermore, the wear rates and the coefficients of friction were lower, at higher milling times due to high densities (96%), and higher elasto-plastic resistance, as presented by the H/E and H^3/E^2 values of 0.026 and 0.0021 GPa, respectively. Increased milling time enables the refinement of grains and reduction in porosity in the Co–Cr–Mo alloy, which in turn increases the alloy's elasto-plastic resistance and enhances its wear resistance.

* Corresponding author.
** Corresponding author.
E-mail addresses: mamoune.fellah@univ-khenchela.dz (M. Fellah), aleksei.obrosov@b-tu.de (A. Obrosov).
https://doi.org/10.1016/j.jmrt.2023.06.031

1. Introduction

Hip prosthesis is an internal joint device [1], the purpose of which is to replace the hip joint and restore it to near-normal function. Thus, the properties of the implant material are critical [2]. The chemical, mechanical, and structural qualities of implants should therefore be optimised and novel biomaterials are to be developed to fulfill these requirements [3,4].

Biomaterials are used in several surgical procedures, such as, hip, knee, dental implants, replacement of arterial segments, skin grafting, etc., and are classified, according to their function and nature, into four different types mainly identified as polymers, ceramics, natural materials, metals and metallic alloys.

In the realm of biomaterials, metallic materials are without a doubt the oldest and most versatile, with the usage of pure materials (gold, silver, platinum) since the early days [5,6]. However, stainless steels that have good corrosion resistance coupled with excellent mechanical properties (stiffness, fatigue strength, and fracture toughness) have lately found their way in biomedical applications [7].

Furthermore, with the advent of technology, a variety of metallic alloys, such as, titanium and titanium alloys, cobalt-chromium alloys, stainless steel, cobalt-chromium-molybdenum alloys, and tantalum have been developed and are being used extensively for metal-based implants. However, among the mentioned metallic alloys, the cobalt-based alloys seem to be a subject of extensive research [8].

These alloys have a wide range of applications in medical devices due to their excellent corrosion resistance (superior to 316L stainless steel), their resistance to allergic reactions when in contact with human tissue (biocompatibility) and appropriate mechanical properties for human activities [9].

The first use of Co–Cr–Mo alloys in the medical field was in dentistry, as removable frames [10]. Over time, the applications of these alloys got diversified, and currently they are widely used in total hip and knee replacements, and for the supports of heart valves [11]. Studies have shown the preference of cobalt-based to titanium-based alloys for joint, metal-to-metal contact applications [12] as their tribological properties are superior to those of titanium alloys. For the Co–Cr–Mo alloy, the chromium provides excellent corrosion resistance by spontaneously forming a thin layer of surface oxide (usually 2–10 nm) in contact with water, which greatly slows the corrosion rate. In order to refine the crystal grains and increase tensile strength, molybdenum is added [13]. The structural and tribological characteristics of the biomaterial are greatly influenced by the manufacturing process.

Thus, casting used for the production of Co–Cr-based alloy molding implants is not a preferred technique, because solidification during casting results in large dendritic grains that decreases the yield strength of the alloy, and cause defects, such as inclusions and micropores that raise internal stresses [14]. Since the last few decades the F75 molded Co–Cr–Mo alloy has been used in orthopedic implants [14,15]. However, in order to ensure adequate homogeneity, reduce the castings' porosity, and enable further mechanical machining, hot isostatic compaction and heat treatments were required [16]. Moreover, the machining of titanium and cobalt alloys is very difficult [17] because of the set of properties that they have in common, in particular, a complex surface integrity [18].

The cast Co–28Cr–6Mo alloy ASTM F75 has excellent mechanical properties and high wear resistance compared to Ti alloys, in addition to their high corrosion resistance compared to the stainless steel 316L especially in human body.

Recently, there has been a great deal of interest in powder metallurgy techniques based on solid-state atomic diffusion [19], which can avoid problems associated with casting, such as the segregation or extensive growth of grains [20,21] and has additional benefits like convenient realization of parts with complex shapes and alloy composition control [22]. However, various factors such as, the formation of homogeneous alloy powders with appropriate particle sizes play an important role in determining the final properties of the developed alloys. Studies have shown that refining alloy particles by high-energy ball milling is beneficial for the sintering process [23].

The current research, is one of the first attempts to investigate the influence of milling time on the structural parameters, mechanical properties and the tribological behavior of a Co–Cr–Mo alloy, by evaluating density, Young modulus, micro-hardness, microstructure, friction and wear resistance.

2. Materials and methods

2.1. Material synthesis

Elemental Co, Cr and Mo powders purchased from Sigma Aldrich Chemicals P Ltd were used for the synthesis of the Co–Cr–Mo alloy. Table 1 below shows the characteristics of the elemental powders.

A mixture of the above elemental powders was prepared in the desired composition (Co–28Cr- 6 Mo), and subjected to a milling process in a high energy ball mill (Fritsch P7) under a protected argon atmosphere for durations of 2, 6, 12 and 18 h respectively. The milling medium consisted mainly of 10 mm diameter alumina balls in an 80 ml vial, using a ball-to-powder ratio of 15:1. Milling was done in 28-min cycles with a 9-min rest period in between. After each milling operation, the vials were opened after a 30–35 min cooling period to avoid excessive heating of the powders by repeated collisions.

The milled powders were cold pressed uniaxially with a hydraulic press and a pressure of 150 MPa to obtain the desired cylindrical shape with a diameter of 13 mm, followed by Hot Isostatic Pressing (HIPed), at a temperature of 1000 °C, under a load of 400 MPa in an argon atmosphere for 45 min. The HIPed samples were finally sintered at a temperature of

Table 1 – Characteristics of as-received elementary Co, Cr, Mo powders.

Element	Co	Cr	Mo
Average size (μm)	<150	<150	<150
Purity (%)	99.8	99.5	99.9
Shape	Irregular	Irregular	Irregular
Melting point (°C)	1493	1857	2617

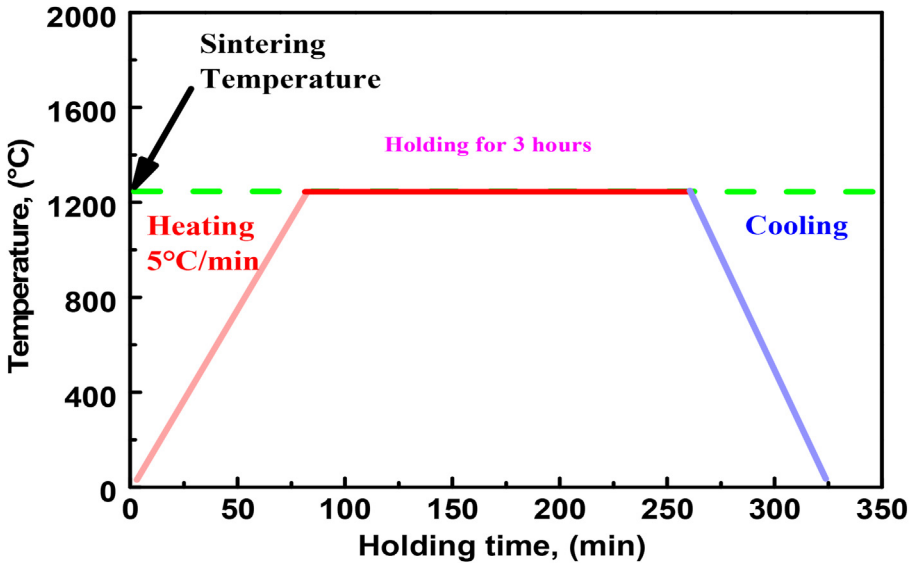

Fig. 1 – The sintering Heat Treatment Cycle of compacted Co–Cr–Mo Alloys.

1250 °C in an inert gas atmosphere, with a heating and cooling rate of 15 °C/min and 20 °C/min, respectively, and a holding time of 3 h. The sintering heat treatment cycle is summarized in Fig. 1.

Fig. 2 summarizes the synthesis and characterization procedure.

2.2. *Material characterizations*

2.2.1. *Structural and mechanical characterization*

Structural characterization was mainly performed using Scanning Electron Microscopy (SEM type Hitachi S-520) and X-Ray Diffraction Analysis (XRD type INTEL CPS 120/Brucker AXS). SEM was used to study the powder morphology, and to analyze the wear mechanisms after the wear tests. XRD was used for structural characterization.

The SEM analyses were carried out with an accelerating high voltage (HV) of 25 KV. XRD analysis was performed with voltage and current values of 40 KV and 20 mA, respectively, and Cu-$_{K\alpha}$ radiation ($\lambda = 1.5406$ Å), in a scan range of 20–110° and a sweep speed of 0.005°/s.

The crystallite size (D) was determined using the Scherrer formula [24]:

$$\beta = \frac{k\lambda}{D\cos\theta} \quad (1)$$

The Williamson Hall equation was used to determine the microstrain ϵ [25];

$$\beta\cos\Theta = 4\,\epsilon\sin\Theta + \frac{K\lambda}{D} \quad (2)$$

Mechanical characteristics such as density, hardness, porosity, elastic modulus and roughness were also evaluated.

The density was measured according to the Archimedean principle in accordance to ASTM D792 standard [26], while the microhardness and Young's modulus were determined with the Vickers's microindenter type ZwickRoell ZHV10 in accordance to ASTM E384 standard. The roughness R_a of the sintered Cr–28Co–6Mo samples was measured with an optical profilometer type VEECO-Wyko q300.

2.2.2. *Tribological characterization*

After Hot Isostatic Pressing and sintering friction tests were carried out using a ball-on-disc Tribotester from TRIBOtechnic as illustrated in Fig. 3, according to ISO 7148, ASTM G- 99, ASTM G181-11, ASTM G119.

All wear tests were performed in a simulated body fluid medium (composition see Table 2).

3. Results and discussion

3.1. *Structural and mechanical characterization*

3.1.1. *Particles size and morphology analysis*

The SEM micrographs of the as received elemental powders of Co, Cr, Mo are shown in Fig. 4. The SEM images confirm the irregular, coarse shape of the elemental powders mentioned in Table 1. From the comparison of the images, it can be seen that the elemental Co powder particles are finer than those of Mo and Cr and have more of a granular shape.

Fig. 5 shows the evolution of the morphology and particle size of the milled Co–Cr–Mo powders. At lower milling times (2 h) as seen in Fig. 5(a), the powder was uniformly distributed over the entire surface. It can be clearly seen that the powder grains are relatively large, with an estimated size of 40–120 μm. With increasing milling time the percentage of fine particles increased, as can be clearly seen in Fig. 5(b) and (c). The size of particles in these cases is about 10–100 μm at a milling time of 6 h and 10–80 μm at a milling time of 12 h, respectively. At a milling time of 12 h, it can clearly be noticed that fine, uniformly dispersed and granular shaped particles dominate.

The same results were documented by F. *Sańchez-De Jesús* et al. in mechanically alloyed Co–28Cr–6Mo using a 1:10 ball-

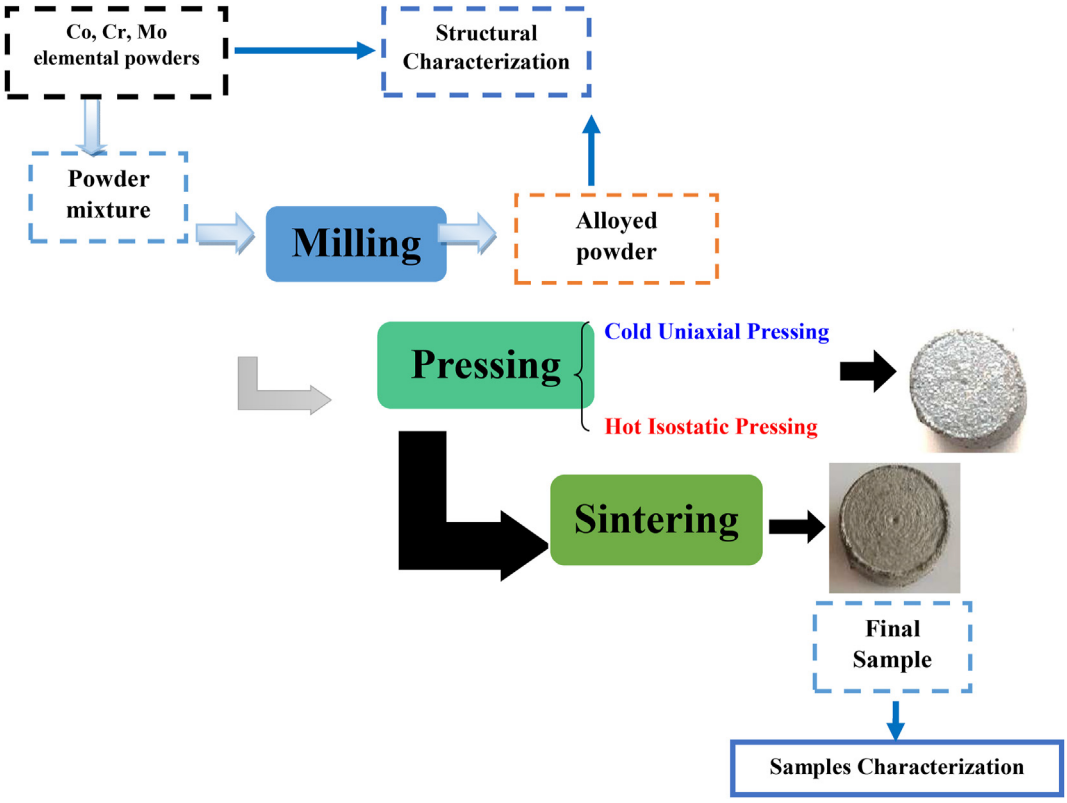

Fig. 2 – Schematic presentation of the synthesis and the characterization procedure.

to-powder weight ratio, by regular milling and pre-alloying, the latter method resulting in homogenous, round particles [28], Furthermore, *Habibe* et al. reported that at a weight ratio of 6:1, the particle of the Co–Cr– Mo–W powder decreases by 50% and the particles tend to spheroidize.

On the other hand, very fine particles (<10 μm) and strong agglomerates were found in the powder sample milled for 18 h, as shown in Fig. 5(d). The occurrence of agglomerates has been mentioned in several studies, e.g., agglomeration in titanium Ti-based alloys synthesized by high-energy ball milling. Likewise, agglomerates were found in powders of Ti–6Al-X alloy synthesized by high duration milling [26,29].

Phenomena like micro-forging, fracturing, agglomeration, and de-agglomeration occur during the high energy ball

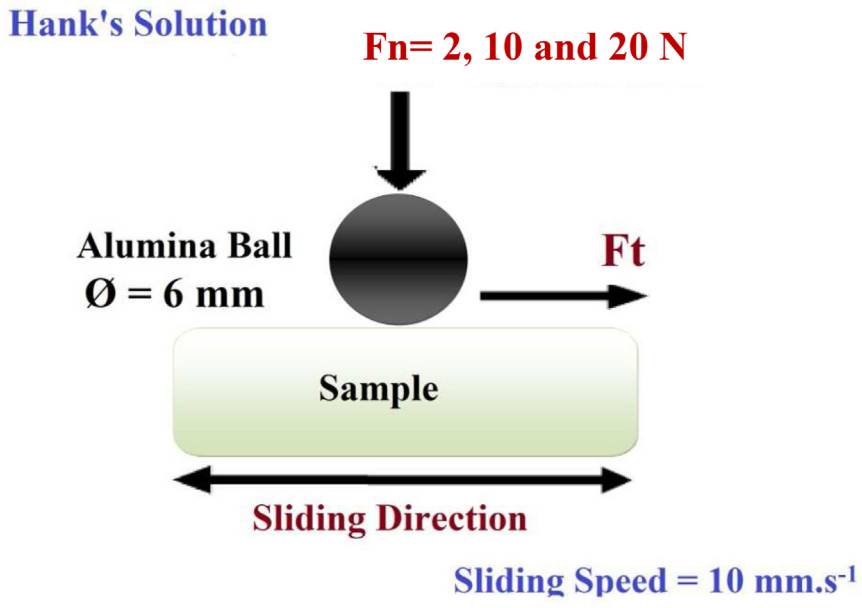

Fig. 3 – Scheme of the tribometer test (type ball on disc).

Table 2 – Composition of Hank's solution [27].

Elements	NaCl	KCl	$CaCl_2$, $2H_2O$	$NaHCO_3$	$MgSO_4$ $7H_2O$	$MgCl_2$	Na_2HPO_4, $2H_2O$	NaH_2PO_4, H_2O	Glucose	Ph
Concentration (g/L)	8.0	0.4	0.19	0.35	0.06	0.19	0.06	0.25	1.0	6.9

milling procedure due to ball-to-powder-to-wall collisions; consequently, micro-forging and fracturing at lower milling times result in irregularly shaped particles, while at high milling times, such as the sample milled for 18 h repeated cold welding occurs, resulting in agglomerates.

The results obtained by EDS analysis of Co–Cr–Mo powders are shown in Fig. 6. The concentrations of Cr, Co, Mo, Mn and C after a milling time of 18 h were 36.55, 31.57, 12.54 and 19.20 at. %, respectively.

3.1.2. *X-Ray diffraction analysis*

The samples were characterized using a Bruker AXS diffractometer, with angles ranging from 20 to 90°, a step width of 0.02° and Cu K α radiation ($\lambda = 1.541$ A).

The XRD patterns of the alloyed powders are shown in Fig. 7(a). After 2 h of milling, the corresponding XRD pattern shows the presence of ϵ-Co and α-Co phases, besides some peaks of Cr and Mo.

The ϵ-Co phase is represented by the peaks of the (111) (211) and (022) planes at $2\Theta = 43°$, 45° and 67°, respectively. For the α-Co phase the peaks of the (212) (220) and (201) planes appear at $2\Theta = 49.5°$, 75.4 and 87°. The presence of Cr and Mo is due to the fact, that these two elements do not dissolve in the cobalt matrix after 2 h of milling. The Cr peak disappears after 6 h of milling, whereas the Mo peak no longer appears after 18 h of milling, which can be explained by the size of these two atoms. Cr has an atomic radius of 1.85 Å and Mo of 2.01 Å. The incorporation of Mo into the Co matrix therefore requires a higher energy than that of Cr, which is why Mo only disappears after 18 h of milling.

The complete disappearance of all peaks except the two peaks of the ϵ-phase at $2\Theta = 44°$ and 45° proves the effectiveness of ball milling in the mechanical alloying of Co, Cr and Mo powders. After 18 h of milling, only the ϵ-hcp peak is dominant, which is due to the complete dissolution of the α-cubic phase and the incorporation of all alloying elements into the cobalt matrix.

In a similar study, *Sańchez-De Jesús* et al. reported that premixing of all elemental powders did not lead to a complete alloying and that the Mo peak did not disappear even after 9 h of milling but always emerged from the solid solution. A complete disappearance of Mo was observed here only with the predoping method when Mo was added in the final stage [28].

Another observation that emerges from Fig. 7(b) is that as the milling time increases, the width of the peak profile increased, which is a result of particle size refinement and milling induced plastic deformation. Simultaneously, a peak shift toward lower angles can be observed. This is due to the

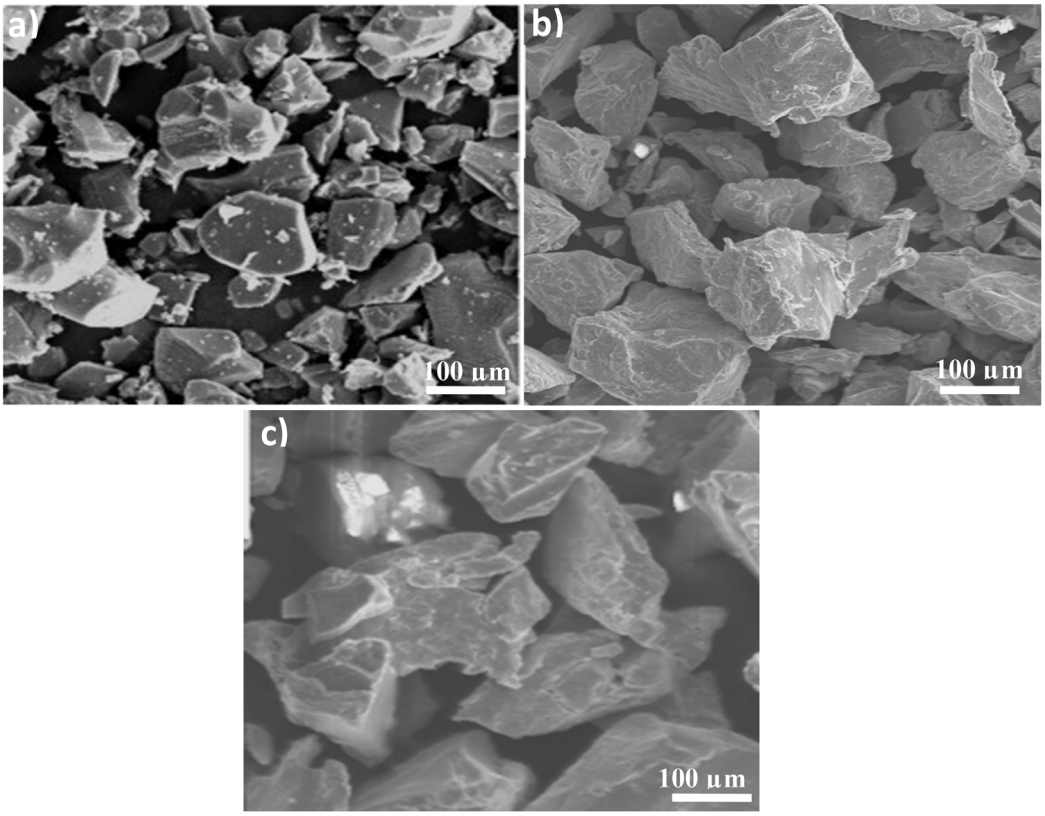

Fig. 4 – SEM images of the as received elemental powders (a)-Co, (b)-Cr and (c)-Mo.

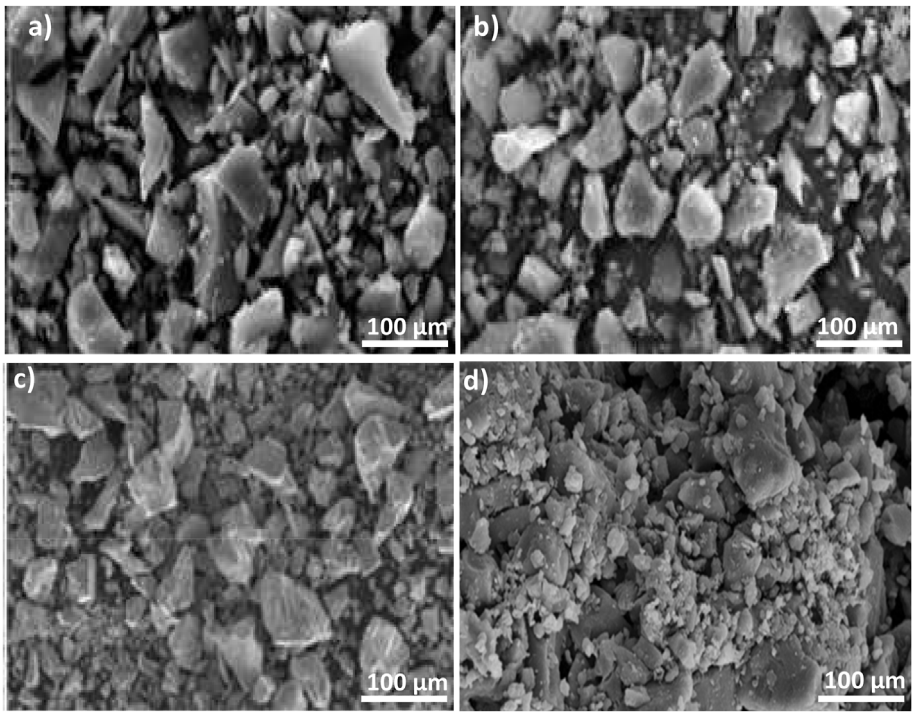

Fig. 5 – SEM images of Co–28Cr–6Mo powders milled for (a) 2h, (b) 6h, (c) 12h and (d) 18h.

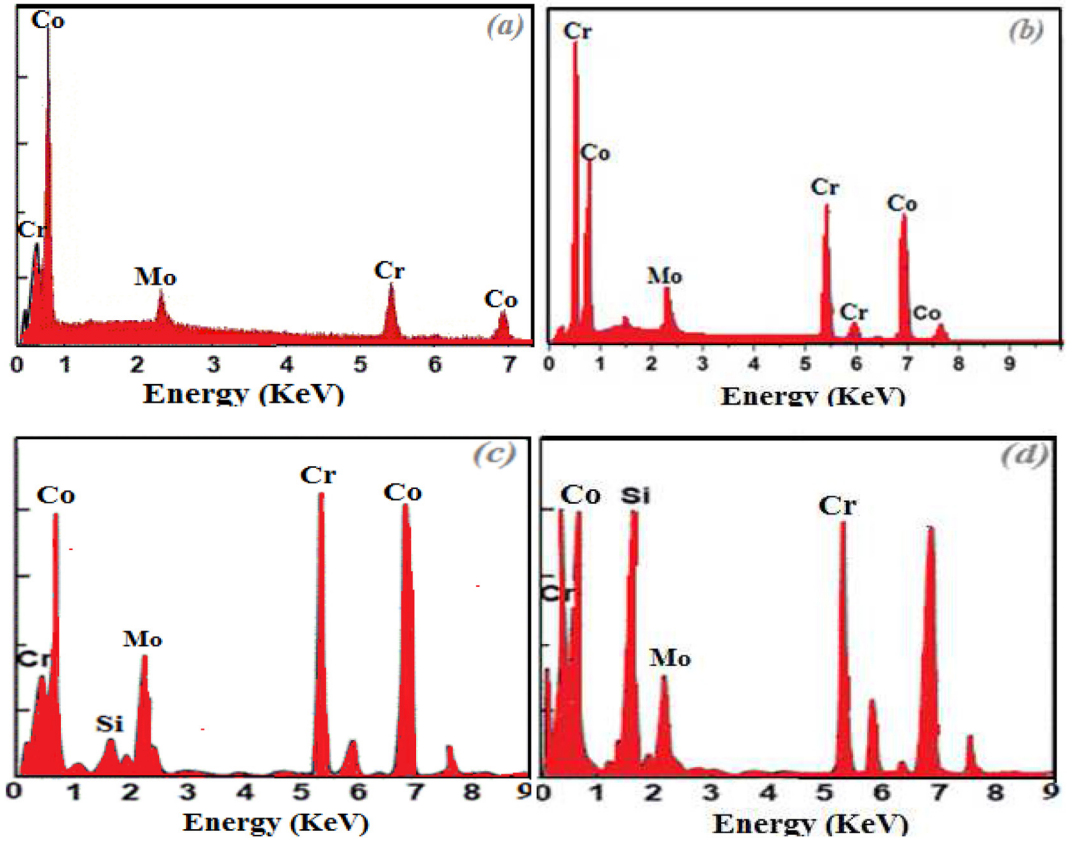

Fig. 6 – EDS spectra of Co–28Cr–6Mo powders milled for (a) 2h, (b) 6h, (c) 12h and (d) 18h.

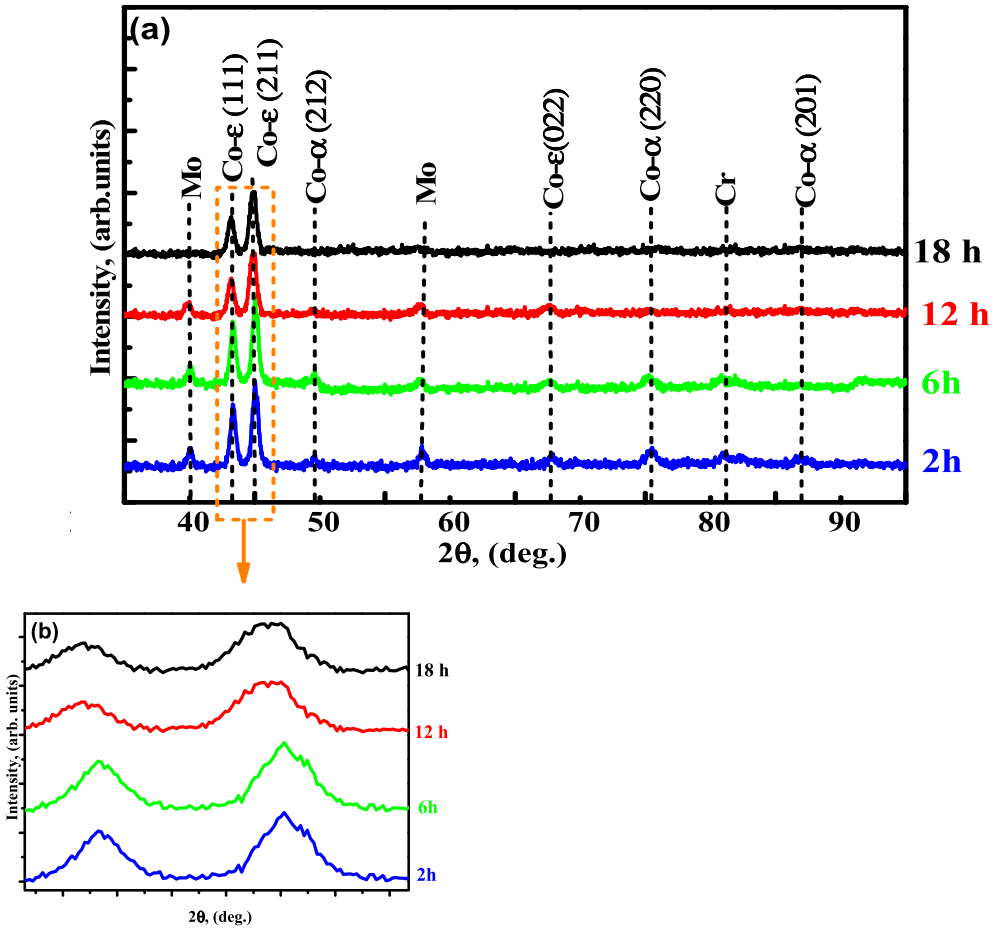

Fig. 7 – (a) XRD patterns of Co–28Cr–6Mo powders milled for 2, 6, 12 and 18 h, (b) Amplification of the XRD patterns showing the shift of the peaks to lower 2Θ angles.

distortion of the crystal structure as a consequence of lattice strain and a variation in the cobalt lattice parameters caused by the incorporation of chromium and molybdenum into the cobalt matrix, especially after 12 and 18 h of milling [28,29].

3.1.3. *Absorbance spectra*

The absorbance was examined for the Co–28Cr–6Mo powders milled for 2, 6, 12 and 18 h within the wavelength range of 198–890 nm. The plot of the absorption ratio as a function of wavelength (Fig. 8) shows, that all doped powders exhibit an increase in absorption with increasing wavelength. It starts with very low values in the ultraviolet wavelengths region of the spectrum between 200 and 400 nm and gradually increases with an increase in wavelength in the visible range between 400 and 700 nm. After that, their values in the infrared region are almost stable. After 2 h of milling, Co–28Cr–6Mo has low absorption, but this increases rapidly with milling time as the absorption of visible light energy increases. Concentrations of Mo and Cr are found in the energy separator, which leads to an increase in absorption and thus a decrease in transmittance.

The increase in milling time of Co–28Cr–6Mo remarkably improves the absorption. Co has an absorption at 235 nm [30], peaks at around 367 and 408 nm correspond to Cr and at 335 nm to Mo [31].

3.1.4. *Grain size distributions*

The particle size distribution is an important parameter to consider for the development of the pore size distribution [32]. The particles should be of different sizes, as in this way it is possible to fill the voids in the larger particle gaps with small particles to increase the fill factor and thus the density of the

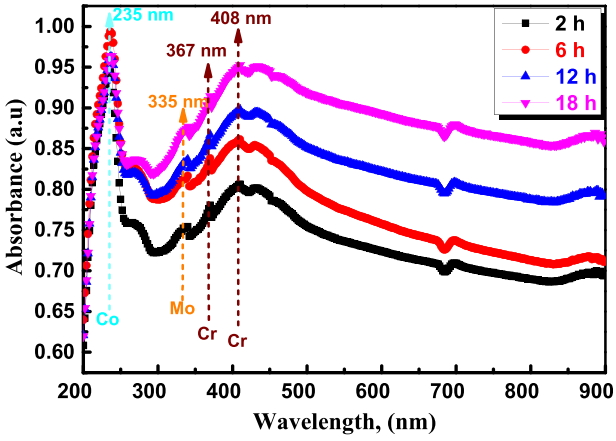

Fig. 8 – UV–Vis Absorption Spectra of Co–28Cr–6Mo powders milled for 2, 6, 12 and 18 h.

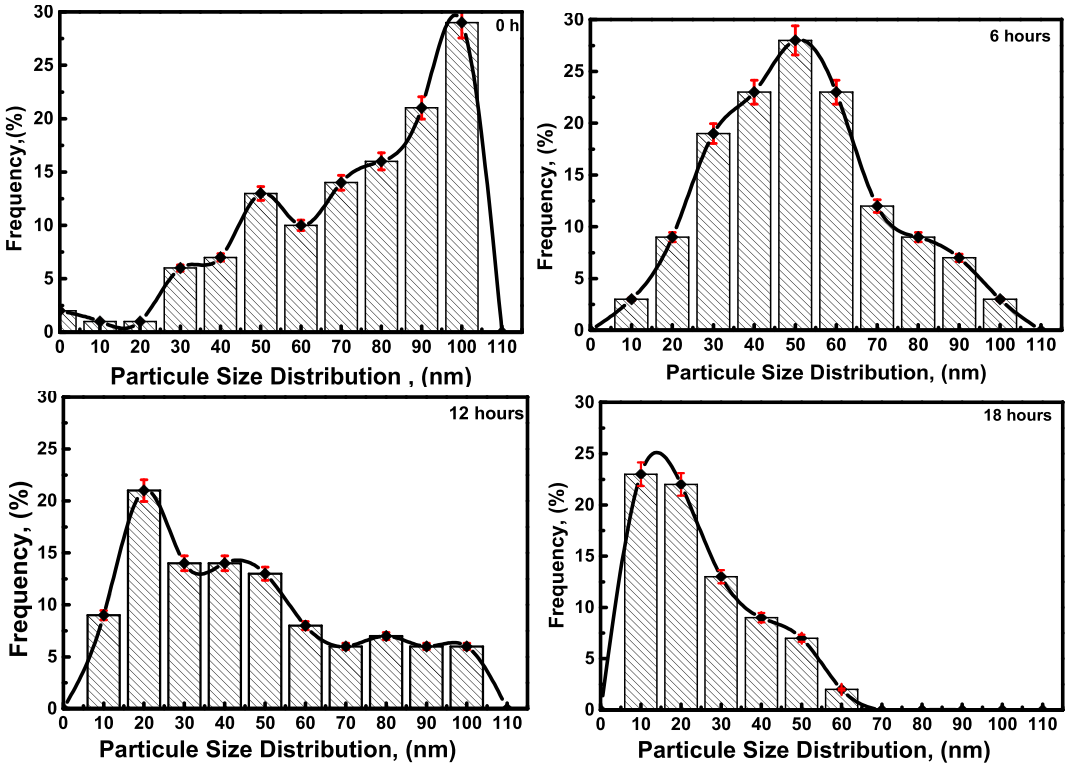

Fig. 9 – Particle-size distribution of milled Co–Cr–Mo alloys at different milling time.

material [33,34]. The pore size decreases with increasing milling time and the density increases accordingly. Before milling (0 h) the majority of the pores were larger than 95 μm. A milling time of 6 h is sufficient to reduce the pore size to 50 nm. Fig. 8 shows that the sample with the highest milling time of 18 h has small, regular pores and a very high density, and the pore size decreases to 15 nm.

Fig. 9 show that the PSD allowed for high packing of the cluster. Moreover, secondary gains associated with this higher density are greater machinability in prosthetic fabrication and potential for orthopedic applications, as well as reduced wear of milling cutters during machining [35].

3.1.5. *Crystallites size and microstrain analysis*

Fig. 10 shows the crystallites size (D), <nm> variation of the Cr–Co–Mo milled powders, as a function of the milling time. It can be clearly seen that the size gradually decreases with increasing milling time, staring from 62 nm for 2 h of milling and reaching a value of 32 nm after 18 h of milling. This evolution is attributed to the fracture caused by increasing milling time, which decreases the particle size and hence resulting in a reduction in the crystallites size [36]. It is also worth noting that despite the agglomerations encountered after 18 h of milling, a decrease in crystallites size is observed, which confirms the effectiveness of milling in reducing grain size and preserving it even with the excessive milling periods.

Fig. 10 also shows the evolution of microstrain <ϵ> as a function of milling time. As clearly seen, it rapidly increases, from 2 to 12 h with values of 0.001–0.0072% respectively. This can be attributed to the stacking defects and the dislocations density caused by the plastic deformations sustained by the powder particles [16,21], grain surface relaxation and most importantly to lattice distortion caused by phase transformation [36].

After 18 h of milling, microstrain increased gradually, unlike the 2, 6 and 12 h of milling cases, reaching the value of 0.0075% after 18 h of milling. This seems to be explained as follows: the energy transferred to small particles is not sufficient to generate more microstrain, hence, further milling won't have a significant influence.

Furthermore, the transformation has entered the stabilization phase and further phase transformation is not possible, since the Co–Cr–Mo alloy is completely formed. The alloying elements Cr and Mo were completely inserted in the Co matrix forming the final hcp phase. So, further milling, induces

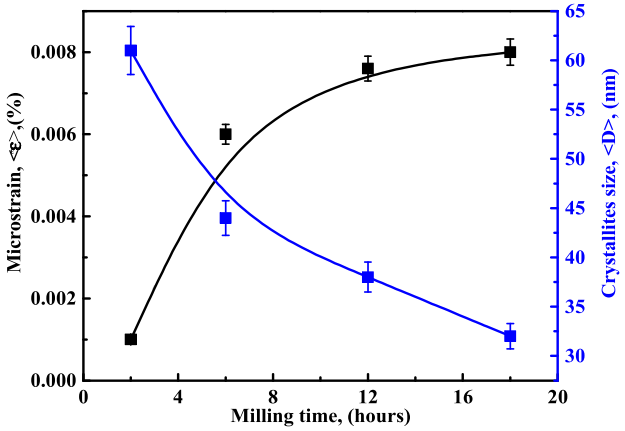

Fig. 10 – The evolution of microstrain <ϵ> and crystallites size <D> with milling time.

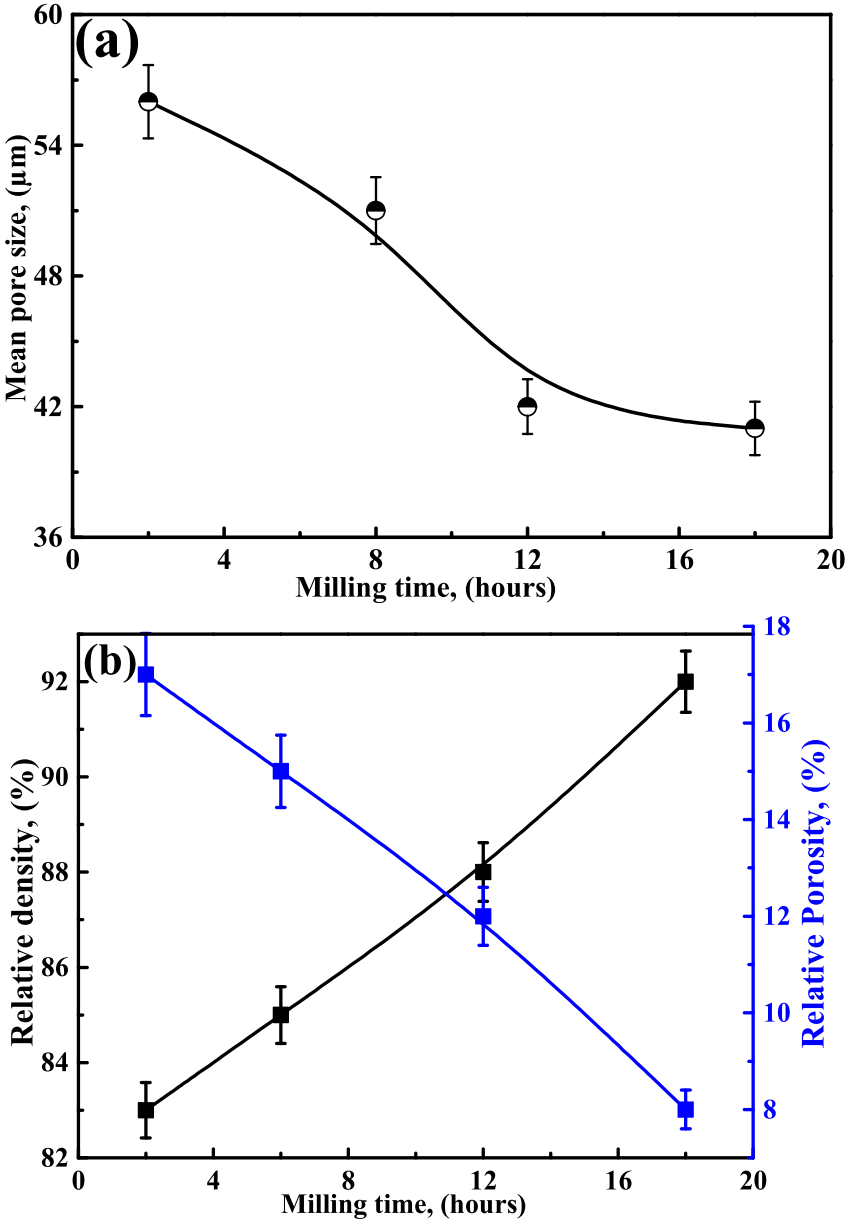

Fig. 11 – Evolution of: (a) of mean pore size (μm), (b) relative porosity (%) and relative density<ρ> (%) of sintered samples with milling time.

further energy that causes lattice distortion which causes the formation of amorphous structures, as reported by *Abada* et al. [37].

3.1.6. *Density and porosity*

The evolution of mean pore size is shown in Fig. 11 (a), in which it can be clearly seen that pore size decreases with increasing milling time. Firstly, from 2 to 12 h, a rapid decrease is observed, however, from 12 to 18 h of milling a gradual decrease is noted. Moreover, it is worth noting that pore size is in the nanometric scale, which confirms the nanostructure of the synthesized material, and the effective choice of synthesis parameters, including pressing loads and sintering temperature and time.

The decrease in pore size is attributed to powder refinement caused by milling; increasing milling time, decreases the particles size of the powders, hence, when compacting, a closed porosity with small pores is obtained.

Similarly, the variation of porosity and density of the alloys synthesized with milled powders is shown in Fig. 11(b), which reveals the proportionality between milling time and density and an inversed proportionality with porosity.

After 2 h of milling, the Cr–Co–Mo density is low with a value of 86% and after 18 h of milling the density is maximum, with a value of 96%, however, porosity is maximum for 2 h of milling with a value of 17% and reaches its minimum value for 18 h of milling. The reason for this evolution is longer milling time which affects the packing of the particles and their

distribution inside the sample during compacting, leading to reduced porosity and high density.

From size consideration, small size particles mean less space between them during compacting, and considering morphology, granular shaped particles caused by high milling time also ensures closed packing during shaping, hence, significantly improving the density [38].

3.1.7. *Young's modulus and hardness*

The Young's modulus of samples is shown in Fig. 12. As presented, A highest value of 200 GPa was obtained for 18 h of milling, and the lowest value of 120 GPa was obtained for 2 h. This can be attributed to the effect of milling time on the cohesion of the material; small particles' size means closed packing and enhanced density, hence cohesion between atoms, consequently, increased stiffness [39].

The Vickers $HV_{0.05}$ micro hardness test for milled materials is also shown in Fig. 11.

As shown in Fig. 12, the hardness increases with increasing milling time. A highest value of 535 $HV_{0.05}$ was obtained for 18h of milling and the lowest value of 335 HV was obtained for 2 h of milling time. This can be accredited to the grain refinement strengthening, caused by decreasing crystallites size and increasing grain boundaries [40].

Takaichi et al. reported a Young's modulus value of 170 GPa and a hardness value of 320 HV for a Co–29Cr–6Mo alloys synthesized by SLP for dental applications [41,42]. These values are closely comparable to values obtained in the present study. Moreover, the Vickers microhardness values of Co-based orthopedic alloys studied by Patel et al. a selective plasma sintering alloy (SPS) were 400, 350 and 850 HV respectively [43]. The synthesized Co–28Cr–6Mo alloy hardness is practically equal to that of ASTM F1537 alloy, which is designed for total joint replacement.

Comparing the mechanical properties of the synthesized Co–28Cr–6Mo alloy with other bio-alloys, it was found that Ti-based alloys: Ti–6Al–4Fe, Ti–Al–7Nb, Ti–15Mo and Ti–15Nb have the following Young's modulus and microhardness values: 110 GPa-350 $HV_{0.05}$ [26], 105 GPa-300 $HV_{0.05}$ [29], 75 GPa-275 $HV_{0.05}$ [27] and 70 GPa-210 $HV_{0.05}$ [24], respectively. This alloy has a high hardness and high Young's modulus, however, to ensure osseointegration, the Young's modulus must be significantly lower, for which additional processing can be performed.

In addition to modulus and hardness other mechanical characteristics such as H/E and H^3/E^2 ratios were also calculated. The variation of H/E and H^3/E^2 ratios as a function of milling time is shown in Fig. 13, which shows that the sample synthesized at 18-h milling has the highest H/E and H^3/E^2 values, indicating its high resistance to plastic deformation [29], which thus increases the wear resistance of the samples. This behavior with respect to elastic and plastic deformation is explained by the increased density and hardening due to grain refinement, respectively, induced by the reduction of the powder particle size as a result of the increased milling period.

3.1.8. *Roughness*

According to *Rosa* et al. For femoral elements of total hip prostheses, spherical bio-implantable metallic materials must have a smooth surface roughness of less than or equal to 0.06 μm. Indeed, the materials used in this study reach Ra values less than 0.5 μm [44,].

Fig. 14 shows the evolution of roughness with milling time of Co–28Cr–6Mo alloy. A significant decrease in Ra values is clearly observed, starting with a value of 8.4 nm for 2 h of milling and reaching 7.2 nm for 18 h milling. This can be attributed to the effect of particles refinement and morphology, fine powders with granular shapes give smooth textures, however, large particles with sharp ends and irregular shapes give smeared textures and high roughness.

Biomedical alloys such as Co–Cr–Mo require certain surface texture to insure its bio-functionality, and osteointegration. Roughness values measured for our alloy are close to that of Co–Cr–Mo generated bone/implant interfacial area by Melentieva et al. who enhanced the surface roughness of a biomedical cobalt based alloy using micro-blasting with aluminum oxide particles [45], yet, the Co–28Cr–6Mo alloy synthesized in the present research doesn't demand additional treatments for improving its surface roughness.

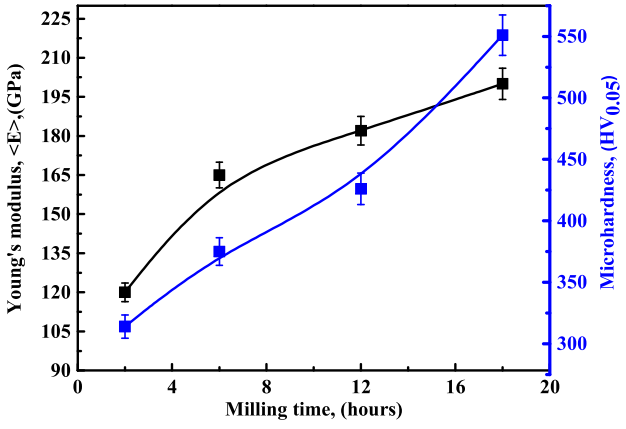

Fig. 12 – Evolution of Young's modulus <E> (GPa) and microhardness $HV_{0.05}$ of Co–Cr–Mo synthesized alloys with milling time.

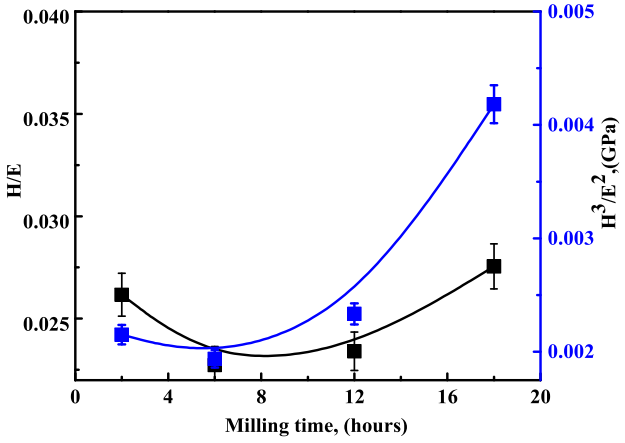

Fig. 13 – Elasto-plastic parameters H^3/E^2 and H/E as a function of milling time.

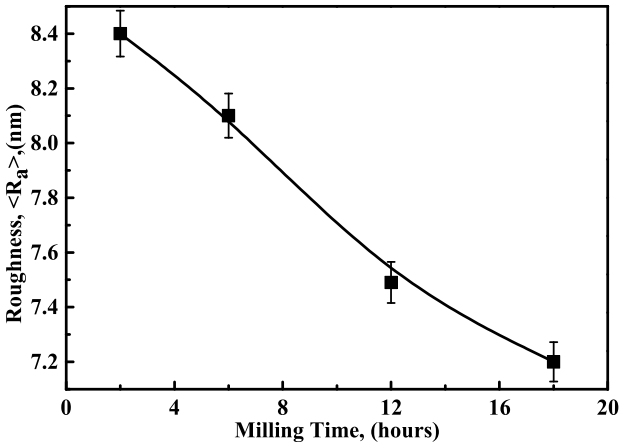

Fig. 14 – The evolution of surface roughness <Ra> (nm) of compacted sintered Co–Cr–Mo alloys as function of milling time.

3.2. *Tribological characterization*

3.2.1. *Mean friction coefficient*

As seen in Fig. 15, the mean coefficient of friction values varied between (0.5 and 0.31) (0.57 and 0.35) and (0.76 and 0.49) for a load of 2, 10 and 20N respectively. It is also clearly observed that the average coefficient of friction values decrease with increasing milling time, which is attributed to the enhanced mechanical proprieties, specifically high hardness, caused by grain refinement, which imposes high loads in order to cause damage by friction. Hence, high milling time results in important resistance to sliding loads. Similar performance was reported by Rezzag et al. for Co–28Cr–6Mo alloy synthesized with different sintering temperatures [46].

It is also worth mentioning that the low coefficient of friction value of the sample synthesized with 18 h of milling confirm the estimation of the elasto-plastic ratios previously presented in Fig. 13, confirming that the elasto-plastic resistance resulted in an enhanced resistance to friction loads.

In similar studies, the coefficient of friction of a Co–28Cr–6Mo alloy synthesized via Metal Injection Moulding (MIM) was found to be 0.52 for 5N load, meanwhile, almost the same value is generated for 10N load (2 h) and 2 N load (12 h) in the present study, the same comparison can be conducted with cast CoCr alloys with a value of 0.55 [47].

3.2.2. *Wear volume and rate*

Wear rate and wear volume were also evaluated after each tribometric test, by measuring the volume of wear traces caused by friction sliding loads.

As shown in Figs. 16 and 17, the wear rate and wear volume decrease with increasing milling time, and increase with increasing loads which reflects and confirms the previously presented mean friction coefficient variation. This can be attributed to the enhanced mechanical proprieties due to grain refinement resulting in improved wear resistance.

The elasto-plastic resistance is the key contributor in reducing wear rate and wear volume, since the surface is resistant to both elastic and plastic deformations caused by sliding loads. In addition tothat, it has been reported that effectively synthesizing Co–Cr–Mo alloys from powders, increases its strength due to grain refinement [48].

Regarding sliding loads, it can be noted that the wear rate for high milling time (18 h and 12 h) is almost the same, which means, increasing load did not have a significant impact on the wear rate due to the reduced roughness, coupled with the accumulation, compaction and probably welding of the wear debris on the surface of the sample may have formed a sort of protective layer causing resistance to wear [46].

The same behavior was reported for various materials synthesized via mechanical alloying, such as in α+β titanium alloys [29] which have superior wear rate and volume values compared to our alloy. In another study, the Mo addition effect on wear was investigated [49], and it was reported that 4 *wt%.* was preferred for high wear resistance. However, in the present study 6 wt%. was forum to be beneficial for higher wear resistance.

Wear volumes of 12, 39 and 3 (*10^6 μm^3) were reported in literature for biomedical cobalt-based alloys; ASTM F75, ASTM

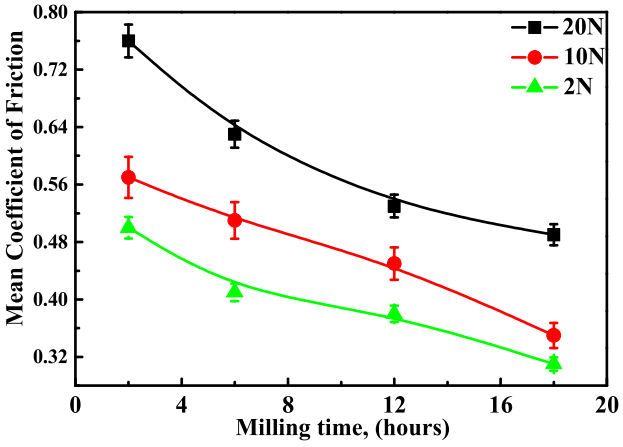

Fig. 15 – The variation of the mean coefficient of friction with milling time.

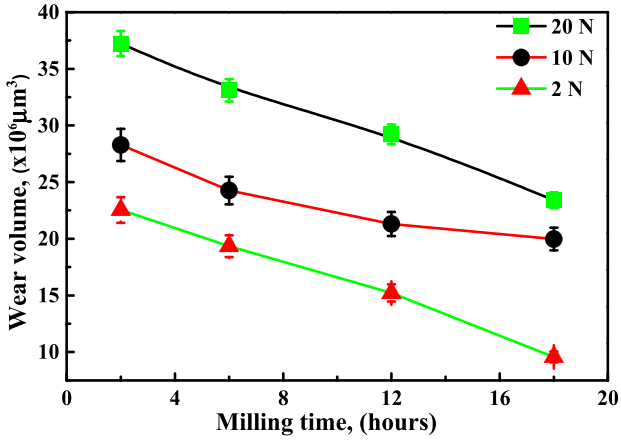

Fig. 16 – The evolution of wear volume (μm^3) according to Milling time and the sliding applied load.

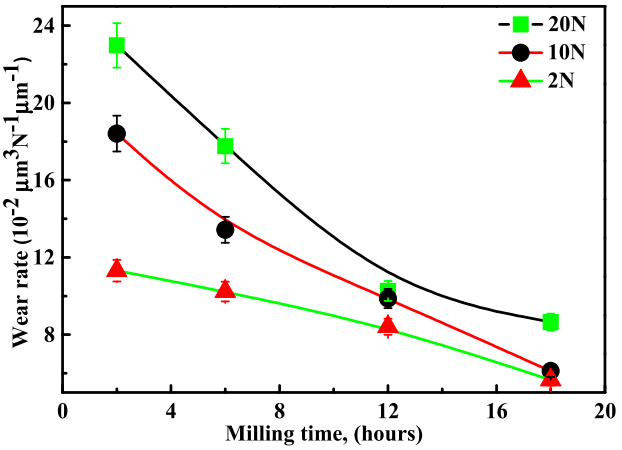

Fig. 17 – The variation of Wear rate (μm^3N^{-1} μm^{-1}) according to milling time and the applied sliding load.

F1537 and SPS alloy respectively [43] for a load of 5N. Hence, the SPS alloy is nearly equivalent to the 18 h sample under 2N load, meanwhile the ASTM F1537 can be equated to the 2 and 6 h milling samples, for 20 N load, for more details see [50–52].

3.2.3. *Wear morphology*

Fig. 18 shows SEM images of the worn surfaces of the Co–28Cr–6Mo alloy synthesized from powders milled for different periods of time. The wear traces are noticeable on the sample with 2 h of milling (Fig. 18(a)). The wear damage is important, because of the pointed roughness of this sample. However, increasing the milling time affected the wear morphologies, in which a reduction of the smeared wear surface can be noticed. In contrast to the sample with 2 h of milling, the finest wear traces are observed in Fig. 16 (d) for the sample synthesized with the highest milling time (18 h), which can be attributed to its high wear resistance caused by the enhanced mechanical proprieties.

The SEM images confirm the previously mentioned hypothesis of increasing wear resistance with the accumulated wear debris. The SEM images clearly show an external layer near the wear traces, in addition to that, the wear volume presented by the size of the wear strips decreases with increasing milling time, which confirms the results previously presented in Figs. 15–17.

As shown in Fig. 18 (a) and (b), wear bands are large so as the size of the grooves, which is attributed to abrasive wear. However, for the sample synthesized from powder milled for 18h, the size of the wear strips decreased, debris are finer and a significant decrease in grooves size is noticed, with a remarkable presence of adhesion, signifying of adhesive wear.

Abrasive wear is caused by the severe damage and detachment of the surface asperities, which are intense in the 2 h milling sample, in contrast to the samples obtained by milling for 18h, that reveals lower surface roughness. In addition, the smooth surface of the worn surfaces corresponds to a low coefficient of friction.

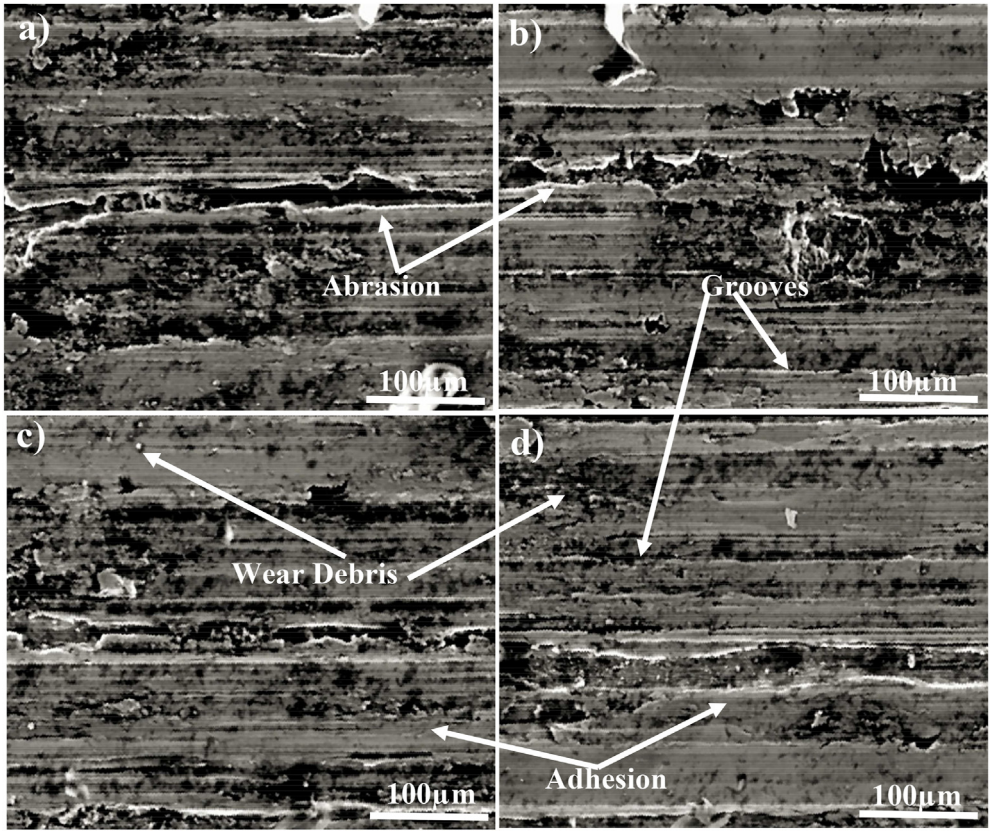

Fig. 18 – SEM images of the worn surfaces of samples with different milling time: (a) 2 h, (b) 6 h, (c) 12 h and (d) 18 h.

4. Conclusion

A Co–28Cr–6Mo alloy was successfully synthesized utilizing high energy ball milling with different milling times, followed by pressing and sintering. Structural, mechanical and tribological characterizations, of the obtained samples were evaluated and the following conclusions can be drawn.

- The structural characterization showed the ability of high-energy ball milling not only in alloying elemental powders but also in downsizing the alloyed mixture and preserving its uniformal dispersion.
- High-energy ball milling is effective for mechanical alloying of powders resulting in a significant reduction in the particle size reaching the value of 15 nm at 18 h milling
- Grain and crystallite sizes of the powders decreased with increasing milling time, reaching low values of <10 nm and 32 nm respectively, at higher milling times, respectively
- Due to grain refinement, atomic cohesion and closed packing, the milled powders exhibited improved mechanical proprieties; higher densities (96%), lower porosities (15 nm), higher hardness (535 $HV_{0.05}$) and stiffness with increasing milling time.
- The absorbance is quickly increases with the milling time, due to the presence of an increase in the absorption of visible light energy to attend the value of 400 and 700 nm
- The enhanced hardness had a significant contribution on improving the tribological performance of the resulting material with the sample prepared with powders after 18 h of milling showed the highest value of hardness 535 $HV_{0.05}$ leading to a significant improvement in wear resistance.
- Wear rates and coefficients of friction decrease with increasing milling times due to high densities (96%), and high elasto-plastic resistance, as can be seen from the H/E and H^3/E^2 values of 0.026 and 0.0021 GPa, respectively
- Abrasive and adhesive wear mechanisms were observed on the worn surfaces depending on the surface texture of the sample.
- Finally, it could be concluded that, improving surface mechanical proprieties and roughness, is the key factor of improving the wear resistance of the material.

Declaration of Competing Interest

The authors declare that they have no known competing financial interests or personal relationships that could have appeared to influence the work reported in this paper.

Acknowledgement

The authors extend their appreciation to the deanship of Scientific Reasearch at King Khalid University for Funding this work through larg group Research Project under grant number RGP2/251/44.

REFERENCES

[1] Hu CY, Yoon TR. Recent updates for biomaterials used in total hip arthroplasty. Biomater Res 2018;22(1):1–12.
[2] Turner CH. Three rules for bone adaptation to mechanical stimuli. Bone 1998;23(5):399–407.
[3] C. Denis and R. A. Menidjel, "Patentability searching for biomaterial and related polymers," World Patent Inf, 34(4) 284–291.
[4] Tranquilli Leali P, Merolli A. Fundamentals of biomaterials. 2009. https://doi.org/10.1007/978-88-470-1195-3_1.
[5] Drotleff S, Lungwitz U, Breunig M, Dennis A, Blunk T, Tessmar J, et al. Biomimetic polymers in pharmaceutical and biomedical sciences. Eur J Pharm Biopharm 2004;58(2):385–407.
[6] Fellah M, Hezil N, Hussein MA, Abdul Samad M, Touhami MZ, Montagne A, et al. Preliminary investigation on the bio-tribocorrosion behaviour of porous nanostructured β-type titanium based biomedical alloy. Mater Lett 2019;257:126755.
[7] Niinomi M. Metallic biomaterials 2008;11(3). https://doi.org/10.1007/s10047-008-0422-7.
[8] Shekhawat D, Singh A, Bhardwaj A, Patnaik A. A short review on polymer, metal and ceramic based implant materials. IOP Conf Ser Mater Sci Eng 2021;1017(1).
[9] Niinomi M. Recent metallic materials for biomedical applications. Metall Mater Trans 2002;333(3):477–86.
[10] Minciuna MG, Vizureanu P, Geanta V, Voiculescu I, Sandu AV, Achitei DC. Effect of Si on the microstructure and mechanical properties of biomedical CoCrMo alloy. Rev. Chim. -Bucharest- Orig. Ed. 2015;66(1):891.
[11] Cartwright R. Book reviews: book reviews. Perspect. Public Health 2010;130(5):239. 239.
[12] Mischler S, Muñoz AI. Wear of CoCrMo alloys used in metal-on-metal hip joints: a tribocorrosion appraisal. Wear 2013;297(1–2):1081–94.
[13] Fellah M, Hezil N, Abdulsamad M, Djellabi R, Montagne A, Mejias A, et al. Effect of molybdenum content on structural, mechanical, and tribological properties of hot isostatically pressed b-type titanium alloys for orthopedic applications. J Mater Eng Perform 2019;28(10):5988–99.
[14] R. Tandon and the International and American Society for Testing and Materials. ASTM, net-shaping of Co-Cr-Mo (F-75) via metal injection molding. ASTM International; 1999.
[15] Nalbant M, Altin A, Gökkaya H. The effect of cutting speed and cutting tool geometry on machinability properties of nickel-base Inconel 718 super alloys. Mater Des 2007;28(4):1334–8.
[16] Fellah M, Hezil N, Abdul Samad M, Touhami MZ, Montagne A, Iost A, et al. The effect of milling time on structural, friction and wear behavior of hot isostatically pressed Ti–Ni alloys for orthopedic applications. Miner. Met. Mater. Ser. 2019:865–75.
[17] Zaman HA, Sharif S, Kim DW, Idris MH, Suhaimi MA, Tumurkhuyag Z. Machinability of cobalt-based and cobalt chromium molybdenum alloys - a review. Procedia Manuf 2017;11:563–70.
[18] Sun J, Guo YB. A comprehensive experimental study on surface integrity by end milling Ti–6Al–4V. J Mater Process Technol 2009;209(8):4036–42.
[19] Munir K, Biesiekierski A, Wen C, Li Y. Powder metallurgy in manufacturing of medical devices. LTD; 2020.
[20] Abidi IH, Khalid FA, Farooq MU, Hussain MA, Maqbool A. Tailoring the pore morphology of porous nitinol with suitable mechanical properties for biomedical applications. Mater Lett 2015;154:17–20.

[21] Ismail MH, Goodall R, Davies HA, Todd I. Porous NiTi alloy by metal injection moulding/sintering of elemental powders: effect of sintering temperature. Mater Lett 2012;70:142–5.
[22] Fellah M, Assala O, Labaïz M, Dekhil L, Iost A. Friction and wear behavior of Ti-6Al-7Nb biomaterial alloy. J Biomaterials Nanobiotechnol 2013;4(4):374–84.
[23] Fellah M, Labaïz M, Assala O, Dekhil L, Taleb A, Rezag H, et al. Tribological behavior of Ti-6Al-4V and Ti-6Al-7Nb alloys for total hip prosthesis. Adv. Tribol. 2014;2014. https://doi.org/10.1155/2014/451387.
[24] Fellah M, Hezil N, Touhami MZ, Obrosov A, Weiß S, Kashkarov EB, et al. Enhanced structural and tribological performance of nanostructured Ti–15Nb alloy for biomedical applications. Results Phys 2019;15:102767. 2019.
[25] Sochacka P, Miklaszewski A, Jurczyk M. Development of β-type Ti-x at. % Mo alloys by mechanical alloying and powder metallurgy: phase evolution and mechanical properties ($10 \leq x \leq 35$). J Alloys Compd 2019;776:370–8.
[26] Hammadi F, Fellah M, Hezil N, Aissani L, Mimanne G, Mechachti S, et al. The effect of milling time on the microstructure and mechanical properties of Ti-6Al-4Fe alloys. Mater Today Commun 2020;27(1).
[27] Fellah M, Hezil N, Dekhil L, Abdul Samad M, Djellabi R, Kosman S, et al. Effect of sintering temperature on structure and tribological properties of nanostructured Ti–15Mo alloy for biomedical applications. Trans. Nonferrous Met. Soc. China (English Ed. 2019;29(11):2310–20.
[28] Sánchez-De Jesús F, Bolarín-Miró AM, Torres-Villaseñor G, et al. Mechanical alloying of biocompatible Co–28Cr–6Mo alloy. J Mater Sci Mater Med 2010;21:2021–6.
[29] Hezil N, Aissani L, Fellah M, Abdul Samad M, Obrosov A, Bokov OD, et al. Structural, and tribological properties of nanostructured $\alpha + \beta$ type titanium alloys for total hip. J Mater Res Technol 2022;19:3568–78.
[30] Okazaki Yoshimitsu, Ishino Akira, Higuchi Shizuo. Chemical, physical, and mechanical properties and microstructures of laser-sintered Co–25Cr–5Mo–5W (SP2) and W–free Co–28Cr–6Mo alloys for dental applications. Materials 2019;12(24):4039.
[31] Okazaki Yoshimitsu, Ishino Akira, Higuchi Shizuo. Chemical, physical, and mechanical properties and microstructures of laser-sintered Co–25Cr–5Mo–5W (SP2) and W–free Co–28Cr–6Mo alloys for dental applications. Materials 2019;12(24):4039.
[32] Xavier de Freitas Bruno, Nunes Carlos Angelo, Santos Claudineidos. Sintering behaviour of Co-28%Cr-6%Mo compacted blocks for dental prosthesis. J Mater Res Technol 2019;8(2):2052–62.
[33] Roudnická Michaela, Kubásek Jiří, Pantělejev Libor, Molnárová Orsolya, Bigas Jiří, Jan Drahokoupil, et al. Heat treatment of laser powder-bed-fused Co–28Cr–6Mo alloy to remove its microstructural instability by massive FCC→HCP transformation. Addit Manuf 2021;47:102265.
[34] Sánchez-De Jesús F, Bolarín-Miró AM, Torres-Villaseñor G, CortéEscobedo CA, Betancourt-Cantera JA. Mechanical alloying of biocompatible Co–28Cr–6Mo alloy. J Mater Sci Mater Med 2010;21:2021–6.
[35] Jiang Feilong, Zhu Weiwei, Zhao Cancan, Li Yulei, Wei Pengbo, Tian Wan, et al. A strong, wear- and corrosion-resistant, and antibacterial Co–30 at.% Cr–5 at.% Ag ternary alloy for medical implants. Mater Des 2019;184:108190.
[36] Hezil N, Fellah M. Synthesis, structural and mechanical properties of nanobioceramic (α-Al_2O_3). Journal of the Australian Ceramic Society 2019;55:1167–75.
[37] Zhao Y, Zhang J. Microstrain and grain-size analysis from diffraction peak width and graphical derivation of high-pressure thermomechanics. J Appl Crystallogr 2008;41(6):1095–108.
[38] Abada A, Bergheul S, Younes A. Mechanical and structural behaviour of TiAlV nanocrystalline elaborated by mechanical milling technique. Micro & Nano Lett 2020;15(14):1023–7.
[39] Hlosta J, Necas J. Effect of particle shape and size on the compressibility and bulk effect of particle shape and size on the compressibility and bulk properties of powders in powder metallurgy. December 2017. 2016.
[40] Chen Y, Burgess T, An X, Mai YW, Tan HH, Zou J, et al. Effect of a high density of stacking faults on the Young's modulus of GaAs nanowires. Nano Lett 2016;16(3):1911–6.
[41] Saba F, Zhang F, Liu S, Liu T. Tribological properties, thermal conductivity and corrosion resistance of titanium/nanodiamond nanocomposites. Compos Commun 2018;10:57–63.
[42] Takaichi A, Nakamoto T, Joko N, Nomura N. Microstructures and mechanical properties of Co – 29Cr – 6Mo alloy fabricated by selective laser melting process for dental applications. J Mech Behav Biomed Mater 2013;21:67–76.
[43] Habibe AF, Fabrício J, Lins C, Simba BG, Magnago RDO, Sá LFD, et al. Co-Cr-Mo-W powder obtained by mechanical alloying. 2020. p. 2–11.
[44] Patel B, Favaro G, Inam F, Reece MJ, Angadji A, Bon W, et al. Cobalt-based orthopaedic alloys : relationship between forming route. microstructure and tribological performance 2012;32:1222–9.
[45] Rosa MB, Albrektsson T, Francischone CE, Schwartz Filho HO, Wennerberg A. The influence of surface treatment on the implant roughness pattern. J Appl Oral Sci 2012;20(5):550–5.
[46] Melentiev R, Kang C, Shen G, Fang F. Study on surface roughness generated by micro-blasting on Co-Cr-Mo. Wear 2019;428–429:111–26.
[47] Rezzag H, Kahloul L, Chadli H, Mebrek A, Saoudi A. Tribological performance and corrosion behavior of CoCrMo alloy. Frat Ed Integrità Strutt 2021;16(59):129–40.
[48] Herranz G, Berges C, Alfonso J, García C, Garrido I. Journal of the Mechanical Behavior of Biomedical Materials Mechanical performance , corrosion and tribological evaluation of a Co – Cr – Mo alloy processed by MIM for biomedical applications. J Mech Behav Biomed Mater 2020;105:103706.
[49] Wang Z, Tang SY, Scudino S, Ivanov YP, Qu RT, Wang D, et al. Additive manufacturing of a martensitic Co–Cr–Mo alloy: towards circumventing the strength–ductility trade-off. Addit Manuf 2021;37:1–14.
[50] Aherwar A, Patnaik A, Bahraminasab M. Effect of molybdenum content on structure and properties of a Co-Cr biomedical alloy. J Mater Eng Perform 2019;28(10):6340–53.
[51] Bouras D, Fellah M, Mecif A, Baril R, Rasheed A Obrosov M. High photocatalytic capacity of porous ceramic-based powder doped with MgO. J Korean Ceram Soc 2023;60:155–68.
[52] Fellah M, Hezil N, Touhami MZ, Abdul Samad M, Obrosov A, Bokov DO, et al. Structural, tribological and antibacterial properties of ($\alpha + \beta$) based Ti-alloys for biomedical applications. J Mater Res Technol 2020;9(6):14061–74.